Appl Phys A (2012) 108:7–11
DOI 10.1007/s00339-012-6981-8

Applied Physics A
Materials Science & Processing

INVITED PAPER

Fabrication and characterization of Al nanomechanical resonators for coupling to nanoelectronic devices

K. Harrabi · Y.A. Pashkin · O.V. Astafiev · S. Kafanov · T.F. Li · J.S. Tsai

Received: 7 May 2012 / Accepted: 7 May 2012 / Published online: 16 May 2012
© Springer-Verlag 2012

Abstract We report on a suspension technique for Al doubly clamped beams. The technique is based on two consecutive reactive ion etching processes in CF_4 plasma, anisotropic and isotropic, of SiO_x on which Al layer is deposited. With this technique, Al doubly clamped beams were fabricated. One of the beams was characterized using a magnetomotive measurement scheme at low temperatures. The developed suspension technique is suitable for the fabrication of Al nanoelectronic devices with a mechanical degree of freedom, in particular, superconducting flux qubits with partly suspended loops.

1 Introduction

Nanomechanichal resonators were in the focus of intensive studies in the past decade for their interesting physics and promising applications [1, 2]. Due to their small size and hence low mass, such resonators are excellent candidates for high-precision mass sensing, with a mass sensitivity approaching one zeptogram [3]. Moreover, their mechanical vibration mode near the quantum limit has attracted a lot of attention. Phonon occupation factors as low as 3.8 have been observed recently [4]. Apparently, one of the biggest challenges in the field is to measure quantum properties of a macroscopic mechanical resonator with a flexural mode and, in particular, detect its ground state. Such measurements were performed recently on a piezoelectric resonator having dilatational modes [5].

Different techniques and methods were used to suspend beams of nanoscale size. Starting from the first demonstration of a Si nanomechanical resonator [6], a number of various materials, mostly single crystal semiconductors and insulators, have been used for the fabrication of resonators [7–11]. Materials, such as silicon carbide and diamond, having a higher group velocity $\sqrt{E/\rho}$, where E and ρ are the Young's modulus and density, give higher resonance frequencies for the same dimensions of the resonators [8, 11], which is favorable for reaching the quantum regime. Typically, the suspension of the resonators is performed as a last step in the fabrication by releasing the patterned film from the underlying sacrificial layer. This is done by using dry etching in chlorine or fluorine based plasma. Also, an organic layer can be used as a sacrificial layer, which can be removed by oxygen plasma [12]. With this approach, metallic nanomechanical resonators are fabricated [13]. Al beams of submicron size deposited on a Si substrate can also be suspended by etching the underlying layer in SF_6 plasma [14]. The use of metallic beams eliminates the metalization step, which is needed in the case of semiconducting and insulating beams, and makes the fabrication process simpler.

Y.A. Pashkin is on leave from Lebedev Physical Institute, Moscow 119991, Russia.

K. Harrabi (✉)
Physics Department, King Fahd University of Petroleum and Minerals, 31261 Dhahran, Saudi Arabia
e-mail: harrabi@kfupm.edu.sa

K. Harrabi · Y.A. Pashkin · O.V. Astafiev · S. Kafanov · T.F. Li · J.S. Tsai
The Institute of Physical and Chemical Research (RIKEN), Wako, Saitama 351-0198, Japan

Y.A. Pashkin · O.V. Astafiev · S. Kafanov · J.S. Tsai
NEC Green Innovation Research Laboratories, Tsukuba, Ibaraki 305-8501, Japan

Y.A. Pashkin
Department of Physics, Lancaster University, Lancaster LA1 4YB, UK

In order to measure the beam in the quantum regime, where the beam fundamental resonance frequency ω_0 has to satisfy the condition $\hbar\omega_0 \gg k_B T$, where $\hbar$ is the Plank's constant, k_B Boltzmann's constant, and T temperature. A few approaches have been pursued including the use of a superconducting transmission line resonator [4, 15] or a high-frequency tank circuit [14] capacitively coupled to the beam. In the latter case, the capacitive coupling can be made strong by reducing the gap between the beam and the driving gate [16]. Some theoretical papers propose qubits as quantum-limited detectors for the displacement of nanomechanical resonators with a flexural resonance mode [17], however, with this scheme the resonator was measured in the classical regime so far [18].

We aim at detecting the ground state of a doubly clamped beam and studying its quantum properties by coupling it to a flux qubit. The qubit will be measured by a dispersive readout as described elsewhere [21]. We have developed a method to fabricate Al high-frequency nanomechanical resonators as doubly clamped beams and integrate them into flux qubits. The suspension technique is based on the deposition of an Al patterned film, either a beam or a flux qubit, on a sacrificial layer through a suspended mask made by electron-beam lithography, and the subsequent removal of the underlying layer using reactive ion etching. In this work, we describe the fabrication process and characterization of an Al beam by the magnetomotive technique. The suspension process includes two successive etching steps, anisotropic and isotropic, in which the RF power and the gas pressure were optimized.

The similarity of our process with the one described in [14] is in using a single gas, however, the gas we used (CF4) is different from the gas (SF6) used in [14]. What is more important is that besides suspending the beam, we made one step further: we incorporated the beam into a flux qubit without affecting its performance. During the etching process the entire chip except for a small window remains protected from the plasma by a resist layer. This may be important in the case when the circuit contains Josephson junctions, which may be affected by the aggressive plasma. The fabrication process of Al beams is fully suitable for nanoelectronic devices fabrication, since most of the superconducting quantum devices are based on Josephson junctions and made of Al (flux qubit, charge qubit, transmon, quantronium, and fluxonium). The beam length was varied between 1 and 30 µm while the width was kept about 100 nm. Transmission of the microwave line with an inserted 4-µm-long doubly clamped beam exhibits a clear frequency dependence with a characteristic dip at the resonance frequency. A few flux qubits with a partly suspended loop were tested at low temperature, however, spectroscopy measurements revealed a bare qubit signal only without any traces of mechanical motion.

2 Fabrication process

The fabrication process starts with the deposition of Al film through a suspended mask formed by electron-beam lithography and dry etching technique. The fabrication details are as follows. A Si wafer covered by a 300 nm-thick layer of SiO_x with the prefabricated 100 nm thick Au contact pads and a coplanar line on top is covered by a tri-layer resist structure as shown in Fig. 1(a). The tri-layer consists of (from bottom to top) a 400 nm-thick copolymer layer, a 30 nm-thick Ge layer and a 50 nm-thick polymethylmethacrylate (PMMA) (see Fig. 1). After the exposure of the top layer in the electron-beam (EB) writer JEOL JBX-5FE and development in a 3:1 mixture of isopropanol (IPA) and methyl-isobutyl-ketone, the pattern in the PMMA is transferred into the Ge layer by reactive ion etching in CF_4. This is followed by the removal of copolymer and undercut creation using oxygen plasma in electron cyclotron resonance etching machine (Anelva, ECR-300). The useful feature of this etcher is that the sample is placed outside the volume in which plasma is generated. This allows more accurate etching control when gas pressure and the incident ion energy are controlled independently. The use of the titling and rotating sample stage and low etching gas pressure gives a possibility to create the desired undercut in the bottom resist layer independently of the exposure dose. Simultaneously, the top PMMA layer is etched away. Finally, a 60 nm-thick Al film is deposited through the mask in the electron-gun evaporator, as shown in Fig. 1(b), which is followed by the

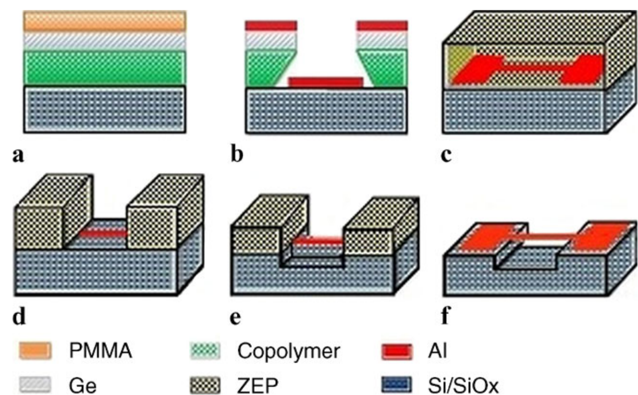

Fig. 1 Schematic diagrams of the fabrication process for an Al nanomechanical resonator: (**a**) Trilayer resist structure built (*from bottom to top*): copolymer/Ge/PMMA; (**b**) Transfer of the beam pattern from the PMMA to Ge layer followed by the undercut creation in an electron cyclotron resonance etching in oxygen. Together with the undercut creation, the top PMMA layer is removed. This is followed by Al deposition in the electron-gun evaporator; (**c**) Positive electron-beam resist ZEP520A-7 spincoated on the wafer; (**d**) A window patterned in the ZEP layer using electron-beam lithography; (**e**) Anisotropic reactive ion etching of SiO_x. The beam remains supported by SiO_x; (**f**) Isotropic reactive ion etching of SiO_x. The beam becomes released from the substrate. See the main text for etching parameters

Table 1 Parameters of two etching steps used in the beam suspension. P is the RF power and p gas pressure

Parameter	P (W)	p (Pa)	Etching time
Step 1: Anisotropic	200	10	1 min 50 s
Step 2: Isotropic	240	240	15 min 30 s

liftoff process in acetone. A similar tri-layer resist structure was used for the fabrication of the flux qubits.

After the beams are formed in Al layer, the wafer is spin-coated with the positive electron-beam resist ZEP520A-7 and baked at 150 °C (Fig. 1(c)). The area surrounding the beam was then exposed in the EB writer and developed in xylene and rinsed in IPA. The developed area forms a window (Fig. 1(d)) through which the SiO_x layer will be subsequently etched away in a CF_4 plasma. We utilized two etching steps: anisotropic process followed by isotropic process. The etching parameters for both processes are listed in Table 1.

Both etching steps were performed in one reactive ion etching machine SAMCO RIE-10NR connected to the CF_4 gas line. The anisotropic etching removes SiO_x leaving almost vertical walls about 80 nm high at the edge of the resist window and beneath the Al beam which acts as a mask (see Fig. 2(a)). During this process, the ZEP resist layer remains practically unchanged.

The anisotropic process is followed immediately by the isotropic process, in order to remove SiO_x beneath the beam and suspend the latter. Besides releasing the beam, this process also creates undercut under the beam clamps as seen in Figs. 2(b) and 3(a), however, this has no effect on the resonator properties for the in-plane vibrations. The remaining ZEP was washed away using an oxygen plasma.

Isotropic etching process leads to the expansion of the pattern created by electron-beam lithography, which is attributed to etching of the resist at the edges. The suspended beams longer than 2 µm tend to buckle, which is caused by the built-in compressive stress in SiO_x. Such beam distortion after the etching process was also seen in earlier experiments [20]. The postbaking of the chip after Al deposition does not have a noticeable effect on the stress. A possible solution could be heating up the chip during the metalization.

3 Measurement

One of the fabricated beams was characterized using the magnetomotive technique [6]. The 4-µm-long beam shown in Fig. 3(a) was placed in a transmission line, mounted in a dilution refrigerator and cooled down to 30 mK. The transmission of the circuit was measured in a perpendicular magnetic field using a network analyzer. The measurement circuit is shown schematically in Fig. 3(a). The high-frequency signal was fed into the transmission line from the output of the network analyzer and received at its input. The alternating current flowing though a conductor placed in transverse magnetic field, generates the Lorentz force that drives the beam parallel to the surface of the substrate (see Fig. 3(a)). This motion in turn generates an electromotive force along the length of the beam resulting in a characteristic dip in the transmission at a resonance frequency, detected by the network analyzer Agilent Technologies E5071C. The resonance frequency of the in-plane fundamental flexural mode of a doubly clamped beam of length L, width w and thickness t can be expressed as [19]:

$$f = \frac{w}{L^2}\sqrt{\frac{E}{\rho}}, \tag{1}$$

where E and ρ are the Young's modulus and the density, respectively.

The beam was measured at the low driving power in the linear regime at different magnetic fields. Figure 3(b) shows a typical resonance curve measured at $B = 3$ T and $T = 100$ mK. For the sake of clarity, the frequency axis is

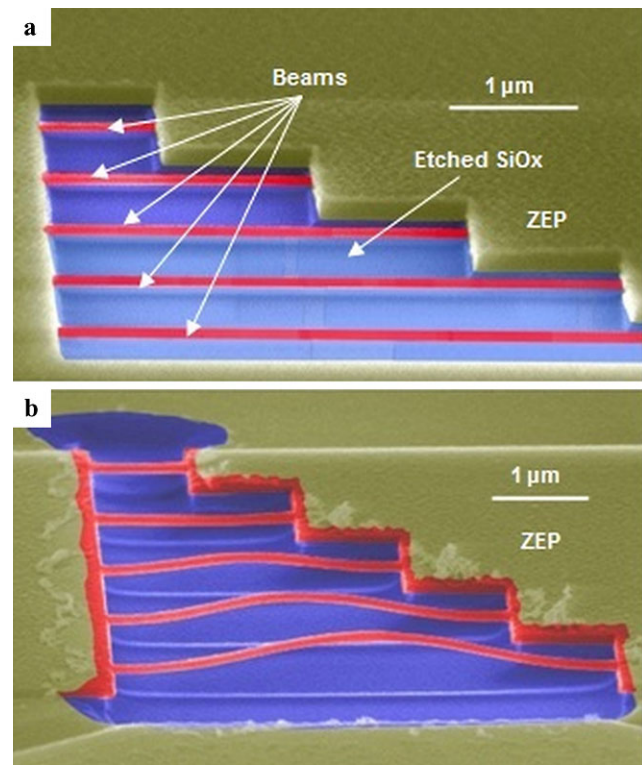

Fig. 2 (**a**) SEM image of five doubly clamped beams after anisotropic reactive ion etching. Al layer remains covered by the ZEP layer. The beams are still supported by SiO_x. (**b**) SEM image of the doubly clamped beams after they were released by combining anisotropic and isotropic process. See Table 1 for the etching parameters. Residues of the ZEP resist are visible on the metal surface. The beams longer than 2 µm tend to buckle due to the compressive stress. (*Inset*) Spectroscopy measurements of 5 µm beam coupled to a flux qubit: frequency of the excited state is plotted vs the current of the magnet.

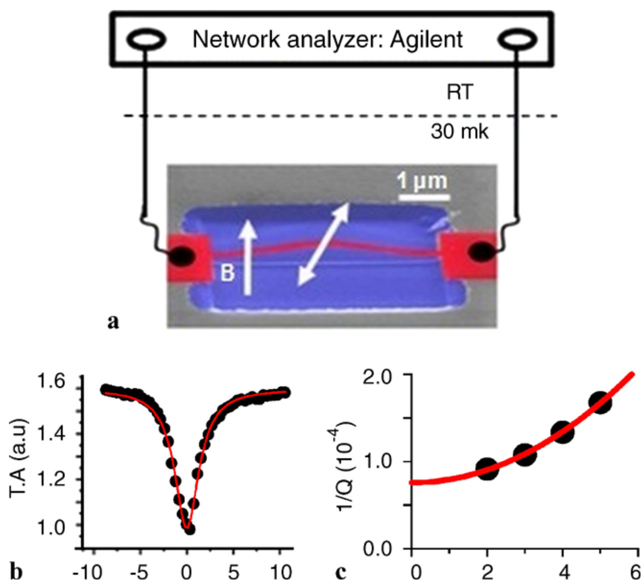

Fig. 3 (**a**) SEM image of the measured Al doubly clamped beam and the measurement setup used to study the suspended beam; (**b**) The resonance frequency dip of the beam measured at 100 mK in a transverse magnetic field of 3 T. The experimental data was fitted with a Lorentzian function, from which the resonance frequency and quality factor were extracted (TA: transmission amplitude). (**c**) Damping $1/Q$ as a function of the applied magnetic field. *Red line* is a parabolic fit to the experimental data

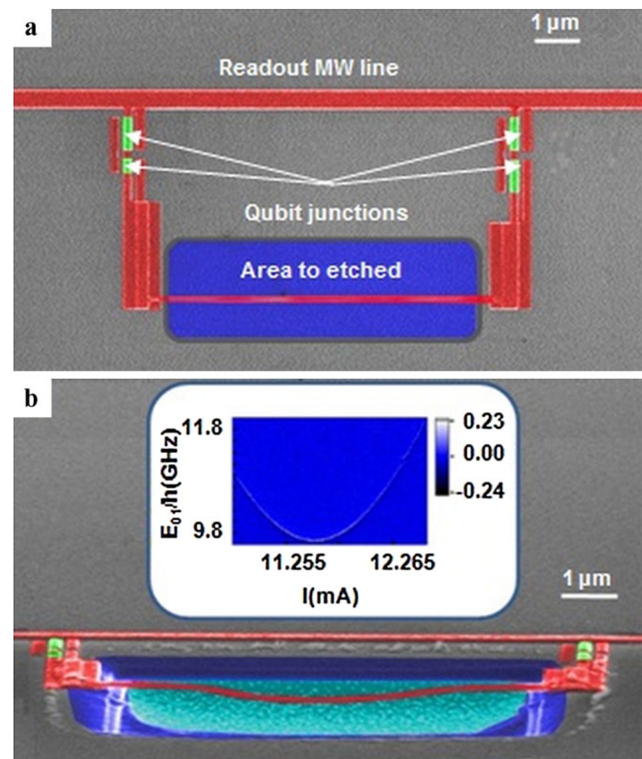

Fig. 4 (**a**) Top view in SEM of the flux qubit, which is a superconducting loop interrupted by four Josephson junctions and part of the loop to be suspended after etching by SiO_x. (**b**) Side view in SEM of the flux qubit with one side of the loop suspended. *Inset*: spectroscopy measurements: the E_{01}/h vs applied current of the magnet

plotted in units of $\Delta f = f - f_0$, where f is the driving frequency and $f_0 = 29.64$ MHz is the measured resonance frequency of the fundamental flexural mode. The Lorentzian fit to the experimental curve, shown as a red line, gives the quality factor $Q(B = 3\text{ T}) = 9300$. Figure 3(c) shows the magnetic field dependence of damping $1/Q$. The extrapolation of this dependence to zero field gives a quality factor $Q = 12\,900$, which is not affected by the magnetomotive losses. As expected, the dependence is parabolic and was observed in earlier experiments with similar beams [6, 13]. In the absence of tension, Eq. (1) gives the resonance frequency of 31.85 MHz, which is about 7.5 % higher than the measured value, apparently due to the remaining compressive stress in the beam. Based on our previous studies, Al beams made using this technique are similar to those made of single crystal materials, such as Si, AlN, and GaAs. In particular, our beams have a high quality factor $\sim 10^4$, which is comparable to what was obtained on other beams made of various materials and fabricated by different processes.

4 Flux qubit with a mechanical degree of freedom

The suspension technique described above was also used to fabricate a flux qubit with a partly suspended loop. The qubit was fabricated first on a Si/SiO_2 substrate using a standard tri-layer resist structure shown in Fig. 1(a). The Ge mask was formed by electron beam lithography and dry etching as described in Sect. 2. The flux qubit was fabricated by two-angle deposition of Al layers through the Ge mask with an oxidation step in between two depositions. The qubit before the beam suspension is shown in Fig. 4(a) together with a blue rectangle in which SiO_x is to be etched away and the beam released in the further processing steps. Following the steps depicted in Fig. 1(c)–(f), the chip was covered by electron-beam resist ZEP520-A, in which a window was opened by electron-beam lithography. Finally, SiO_x was etched in two steps in the RIE machine to release the beam. The side view of the qubit with a suspended beam is presented in Fig. 4(b). The qubit is coupled to the microwave transmission line for the dispersive measurements [21]. The idea of the future experiment is to measure quantum properties of the nanomechanical resonator having a fundamental bending mode frequency exceeding $k_B T$. We did spectroscopy measurements on several flux qubits having a nanomechanical resonator built into the qubit loop.

Spectroscopy data for a 5 μm beam coupled to a flux qubit is shown in the inset of Fig. 4(b), which confirms that the qubit worked properly. From this data, we deduced the qubit splitting energy $\Delta = 9.65$ GHz and persistent cur-

rent $I_p = 190$ nA. These parameters are very close to the designed ones and similar to the values reported in [22]. Nonetheless, the vibration mode was not detected. We believe that the main reason for this was the weak resonator–qubit coupling. The coupling term is proportional to the dc magnetic field threading the qubit loop, which due to technical constraints was limited to below 1 mT only. In the future experiments, the coupling will be increased ten times by the tenfold increase the applied dc magnetic field.

5 Conclusion

In conclusion, a combination of anisotropic and isotropic processes in RIE CF_4 plasma was used to suspend Al doubly clamped beams. One beam was characterized at low temperature using a magnetomotive measurement technique. We found out that the results were as good as those obtained using different techniques. This method was used to introduce a mechanical degree of freedom to the superconducting flux qubit by partly suspending the qubit loop. The fabricated circuit will be used in the experiments aimed at detecting the quantum states of the flexural nanomechanical resonator.

Acknowledgements This work was supported by the JSPS through its FIRST Program and MEXT kakenhi "Quantum Cybernetics". K.H. gratefully acknowledges the support of the King Fahd University of Petroleum and Minerals, Saudi Arabia, under the FT100009 DSR project.

References

1. K.L. Ekinci, M.L. Roukes, Rev. Sci. Instrum. **76**, 061101 (2005)
2. K.C. Schwab, M.L. Roukes, Phys. Today **58**, 36 (2005)
3. Y.T. Yang, C. Callegari, X.L. Feng, K.L. Ekinci, M.L. Roukes, Nano Lett. **6**, 583 (2006)
4. T. Rocheleau, T. Ndukum, C. Macklin, J.B. Hertzberg, A.A. Clerk, K.C. Schwab, Nature **463**, 72 (2009)
5. A.D. O'Connell, M. Hofheinz, M. Ansmann, R.C. Bialczak, M. Lenander, E. Lucero, M. Neeley, D. Sank, H. Wang, M. Weides, J. Wenner, J.M. Martinis, A.N. Cleland, Nature **464**, 697 (2010)
6. A.N. Cleland, M.L. Roukes, Appl. Phys. Lett. **69**, 2653 (1996)
7. R.G. Beck, M.A. Eriksson, R.M. Westervelt, Appl. Phys. Lett. **73**, 1149 (1998)
8. Y.T. Yang, K.L. Ekinci, X.M.H. Huang, L.M. Schiavone, M.L. Roukes, C.A. Zorman, M. Mehregany, Appl. Phys. Lett. **78**, 162 (2001)
9. A.N. Cleland, M. Pophristic, I. Ferguson, Appl. Phys. Lett. **79**, 2070 (2001)
10. L. Sekaric, D.W. Carr, S. Evoy, J.M. Parpia, H.G. Craighead, Sens. Actuators A **101**, 215 (2002)
11. L. Sekaric, J.M. Parpia, H.G. Craighead, T. Feygelson, B.H. Houston, J.E. Butler, Appl. Phys. Lett. **81**, 4455 (2001)
12. T.F. Li, Yu.A. Pashkin, O. Astafiev, Y. Nakamura, J.S. Tsai, H. Im, Appl. Phys. Lett. **91**, 033107 (2007)
13. T.F. Li, Yu.A. Pashkin, O. Astafiev, Y. Nakamura, J.S. Tsai, H. Im, Appl. Phys. Lett. **92**, 043112 (2008)
14. M. Sillanpää, J. Sarkar, J. Sulkko, J. Muhonen, P.J. Hakonen, Appl. Phys. Lett. **95**, 011909 (2009)
15. C.A. Regal, J.D. Teufel, K.W. Lehnert, Nat. Phys. **4**, 555 (2008)
16. J. Sulkko, M. Sillanpää, P. Häkkinen, L. Lechner, M. Helle, A. Fefferman, J. Parpia, P.J. Hakonen, Nano Lett. **10**, 4884 (2010)
17. A.D. Armour, M.P. Blencowe, K. Schwab, Phys. Rev. Lett. **88**, 148301 (2002)
18. M.D. LaHaye, J. Suh, P.M. Echternach, K.C. Schwab, M.L. Roukes, Nature **459**, 960 (2009)
19. H.W.Ch. Postma, I. Kozinsky, A. Husain, M.L. Roukes, Appl. Phys. Lett. **86**, 223105 (2005)
20. S. Etaki, M. Poot, I. Mahboob, K. Onomitsu, H. Yamaguchi, H.S.J. van der Zant, Nat. Phys. **4**, 785 (2008)
21. O. Astafiev, A.M. Zagoskin, A.A. Abdumalikov Jr., Yu.A. Pashkin, T. Yamamoto, K. Inomata, Y. Nakamura, J.S. Tsai, Science **327**, 840 (2010)
22. F. Yoshihara, K. Harrabi, A.O. Niskanen, Y. Nakamura, J.S. Tsai, Phys. Rev. Lett. **97**, 167001 (2006)